The Journal of Experimental Biology 209, 4533-4545
Published by The Company of Biologists 2006
doi:10.1242/jeb.02552

Response characteristics of visual altitude control system in *Bombus terrestris*

Kensaku Tanaka* and Keiji Kawachi

Department of Aeronautics and Astronautics, the University of Tokyo, 7-3-1 Hongo, Bunkyo-ku, Tokyo 113-8656, Japan

*Author for correspondence (e-mail: tanaka@kawachi.rcast.u-tokyo.ac.jp)

Accepted 8 September 2006

Summary

Frequency response characteristics of bumblebees to vertical visual oscillations were measured and analyzed. We measured the vertical force of the bees at four oscillation frequencies (0.9, 1.8, 3.6 and 7.4 Hz), and summarized their response characteristics in terms of amplitude and phase differences. The amplitude was almost constant throughout the examined frequency domain, whereas the phase gradually lagged with increasing frequency. In order to view the relationship between the input (visual oscillation) and output (response of the bee) more clearly as a control system, we compared them in the same dimension; we calculated hypothetical positions of the tethered bees on the basis of the measured variation in the vertical force, and compared them with the visual stripe positions. The resultant gain and phase data were plotted on a Bode plot. A transfer function was identified from the Bode plot, revealing that the response characteristics of the measured system could be represented as a simple expression.

The dynamic control characteristics of the bumblebees were analyzed on the basis of the frequency response data. First, we showed that the measured system possesses a substantial stability margin. This means that the control system has substantial damping characteristics, and was suitable for stable flight control. In addition, our results showed that the measured bumblebee system possesses superior steady state and quick-response characteristics in comparison with a human pilot-vehicle system. Such excellence in both the steady state and transient characteristics (i.e. damping and quick response characteristics) provide the evidence that bumblebees can effectively control their flight with stability and maneuverability.

Key words: bumblebee, *Bombus terrestris*, flight, frequency response, visual oscillation, altitude control, vertical force, Bode plot, transfer function, dynamic stability.

Introduction

Flying insects satisfy both their maneuverability and stability requirements by continuously varying their wing kinematics. Smaller objects have, in general, difficulty in controlling their flight with stability, because they have lower moments of inertia and are more sensitive to high frequency disturbances. The control system must therefore possess sufficient steady state and transient characteristics. Although basic flight mechanisms of insects have been summarized (e.g. Azuma, 1992) and correlations between wing kinematics and aerodynamic force generation have been extensively studied (Lehmann and Dickinson, 1997; Lehmann and Dickinson, 1998; Sane, 2003), the dynamic flight performance has not been studied thoroughly.

Studies on dynamic flight stability of the desert locust *Schistocerca gregaria* (Taylor and Thomas, 2003) provided the first quantitative analysis of dynamic stability of a flying animal. Taylor and Thomas measured the longitudinal static stability derivatives and mass distribution of the desert locusts, and solved the longitudinal equations of motion by utilizing a classical linearized framework of aircraft flight analyses. In the same framework, Sun and Xiong studied the longitudinal dynamic flight stability of a hovering bumblebee (Sun and Xiong, 2005). They computed the aerodynamic derivatives by means of computational fluid dynamics, and solved the equations of motion by eigenvalue and eigenvector analyses. Both studies succeeded in identifying three natural modes of the longitudinal flight: one unstable oscillatory mode, one stable fast subsidence mode, and one stable slow subsidence mode. Neither of them, however, succeeded in explaining the flight stability fully, because of the unstable oscillatory mode.

In the present study, we suggest another approach for the dynamic flight control analysis. Instead of solving the equations of motion to identify the natural modes, we focused on visual altitude control in the flight of a bumblebee *Bombus terrestris*, and on its dynamic control performance. We can evaluate such performances on the basis of a transfer function, which is a mathematical representation of the relation between the input and output of a linear time-invariant system (Franklin et al., 2002). We utilized the frequency response method to

obtain the transfer function for the bumblebee system. The input of the frequency response measurements was a visual oscillation in the vertical direction, which elicited vertical flight modulation from a tethered bumblebee. The output was the vertical force variation of the bee, measured by using a load cell. The oscillation frequency of the input was varied at 0.9, 1.8, 3.6 and 7.4 Hz. We summarized the frequency response characteristics in terms of amplitude and phase differences, and showed them on a Bode plot. The transfer function of the visual altitude control system was identified from the plot. Our results revealed that the measured control system possessed a substantial stability margin, equivalent to that of a human pilot-vehicle system (McRuer and Graham, 1964). In addition, the bumblebee system was revealed to be superior to the human pilot-vehicle system in terms of both steady state and quick-response characteristics. These results provide the evidence that bumblebees can effectively control their flight with stability and maneuverability.

Materials and methods

Insects and their preparation

Bumblebees *Bombus terrestris* L. were chosen as the model insect because of their general availability, and noted flight capability. We obtained colonies of the bumblebees from a commercial supplier (Arysta LifeScience Corporation, Tokyo, Japan). The environment in which the colonies were placed and experiments were performed was maintained at around 20°C, when the bees are fully active. Only female bumblebees were selected because females are larger and more robust than males. We used a total of 12 bumblebees for the measurements, all 1–2 cm long and 1.5–2.5 mN in weight.

In preparation for each experiment, we captured a bee in a Petri dish from the colony, and cooled the dish with ice for approximately 30 min. While the bee was anesthetized at that cold temperature, an iron wire 2.5 cm long×0.7 mm diameter (1 mN weight) was glued to the bee near the characteristic yellow line on its thorax. Although all the bees recovered from the anesthesia within a few minutes, some were inactive for nearly 1 h. We used the bees for experiments after they seemed to be fully active, usually within 2 h.

Stimulus presentation

The family of bees has highly developed eye optics (Spaethe and Chittka, 2003) that are sensitive to image motion (Srinivasan et al., 1999). We utilized this characteristic, and elicited vertical flight modulation from the bumblebees by means of vertical image motion. This technique has mainly been used with flies for some time (e.g. Götz and Wehrhahn, 1984).

We prepared a flight arena, as shown in Fig. 1A, for the purpose of stimulus presentation. This arena shaped a hexagonal cylinder, which is 19.2 cm high, and each side of whose hexagon is 9.6 cm wide. Fig. 1B shows the magnified view of one wall of the arena. The inside wall contained 16 rows of 5.5 mm-diameter LEDs (DU-256N-64C, Azuma Electric, Tokyo, Japan, LED color: orange, wavelength: 610 nm) in the horizontal direction, and 32 in the vertical direction. Horizontal stripe patterns were displayed by lighting alternate 8 rows of LEDs, that is, the period of the stripes was 88 mm. Those stripes were visually oscillated in the vertical direction by using a computer control.

During the experiments, we placed a tethered bumblebee in the middle of the arena, and showed it the visual oscillation.

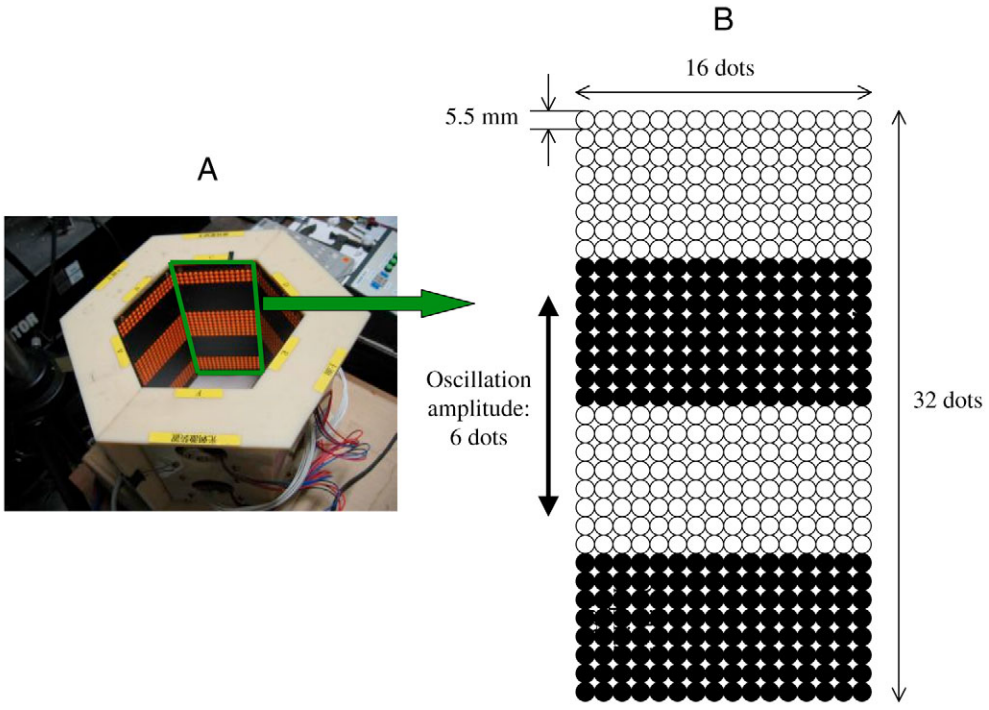

Fig. 1. (A) The flight arena. During the experiments, the bumblebee was fixed inside this arena, and was given a visual stimulus in the vertical direction. (B) Magnified view of one wall of the arena. The inside wall contains 16 rows of LEDs in the horizontal direction, and 32 in the vertical direction. The diameter of each LED is 5.5 mm. We displayed horizontal stripe patterns by lighting alternate 8 rows of LEDs, that is, the period of the stripes was 88 mm. Those stripes were visually oscillated in the vertical direction by using a computer control. The oscillation amplitude was kept constant at 33 mm (6 dots of the LEDs), whereas the oscillation frequency was varied at 0.9, 1.8, 3.6 and 7.4 Hz (i.e. 5.6, 11, 22 and 46 rad s^{-1}).

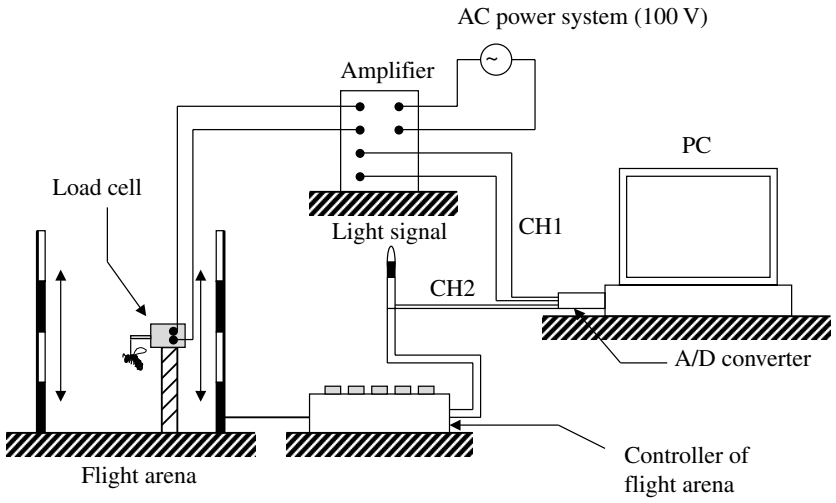

Fig. 2. The measurement system. We measured the vertical force of the bumblebee using a load cell. This load cell was hard-wired to an amplifier using a 100 V AC power system. The output signal was digitalized by an A/D converter, and then stored on a PC. The output signal of the amplifier was imported as channel 1 (CH1). We used a light signal to identify the visual stripe motion, whose output was imported as channel 2 (CH2). This light signal circuit was connected to the flight arena controller. The phase and frequency of the visual oscillation were identified using the CH2 waveform, which enabled us to synchronize the data of the input (visual oscillation) and the output (force variation).

We could verify that the bee was responding to the visual stimulus because the wingbeat sound varied continuously according to the visual oscillation. In other words, the amplitude of the sound oscillated at the same frequency as the stripe motion. Although some bees stopped flapping their wings within a few seconds after the stimulus was given, other bees remained responsive. In the analysis, we used data from the responsive bees. The oscillation frequency of the stripes (ω) was varied at 0.9, 1.8, 3.6 and 7.4 Hz, while the amplitude was kept constant at 33 mm (i.e. 6 dots of LEDs).

Vertical force measurement

Our measurement system is shown in Fig. 2. The vertical force generated by the bee was measured using a load cell (UL-10GR, Minebea Co., Tokyo, Japan). The iron wire glued to the bee was rigidly attached to the load cell with a clamp (8.5 mN weight). This load cell was hard-wired to an amplifier (CSA-507B, Minebea Co.), using a 100 V AC power system. The output signal was digitalized using an A/D converter (NR110, KEYENCE, Osaka, Japan) and stored on a PC. The resonance frequency of the force measurement system was approximately 60 Hz in our experimental conditions, and is much higher than the visual oscillation frequency (at most 7.4 Hz) and lower than the wingbeat frequency (typically 150–200 Hz). The resonance in this force measurement system, therefore, was not coupled with the measurement data. The sampling frequency of the A/D converter was 2 kHz. We recorded the signals for enough time to observe more than one cycle of the visual oscillation in each experiment. The output signal of the amplifier was imported as channel 1 (CH1). We used a light signal to identify the visual stripe motion, whose output was imported as channel 2 (CH2). This light signal circuit was connected to the controller of the flight arena. The phase and frequency of the visual oscillation were identified from the CH2 waveform, which enabled us to

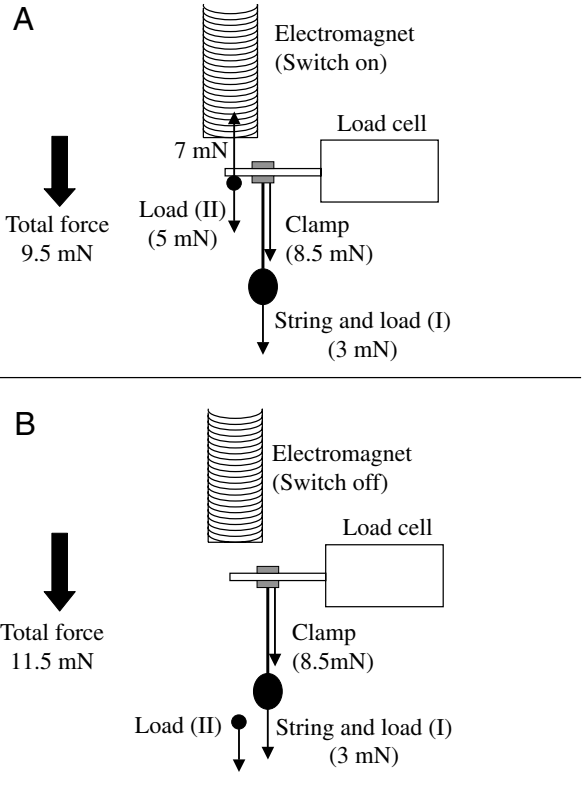

Fig. 3. The dynamic properties of the force measurement system were verified by measuring the step response. (A) Before the step input. A 3 mN weight [load (I)] was loaded on the load cell, for the purpose of adjusting the weight condition to the experiments. In addition, a 5 mN weight [load (II)] and an electromagnet were prepared. Load (II) was iron, and pushed up the load cell by the magnetic force of the electromagnet. The magnetic force worked on load (II) was approximately 7 mN. Note that the magnitude of the additional force does not have an influence on the step response result. (B) After the step input. When the electromagnet was switched off, load (II) was immediately detached from the load cell, which signified the step input. Variations in the voltage of the electromagnet circuit and the output of the force measurement system were recorded at a sampling frequency of 10 kHz.

synchronize the data of the input (visual oscillation) and the output (force variation).

Calibration of dynamic properties of the force measurement system

A proper analysis of the dynamic force measurement data requires a proper correction for the dynamic properties of the force measurement system, which we verified by measuring the step response characteristics (Fig. 3A,B). First, we loaded a 3 mN weight on the load cell [load (I) in Fig. 3A], for the purpose of adjusting the weight to our experimental condition; the total weight of the bee and the wire was approximately 3 mN on average. Next, we prepared a 5 mN weight [load (II)] and an electromagnet. Load (II) was made of iron, and pushed up the load cell by the magnetic force of the electromagnet. The additional upward force was approximately 2 mN, that is, the magnetic force worked on the load (II) was approximately 7 mN. We notify that the magnitude of the additional force does not have an influence on the step response result. Finally, we switched off the electromagnet (Fig. 3B). Load (II) was immediately detached from the load cell, which signified the step input. We recorded the variations in voltage of the electromagnet circuit and the force measurement system (i.e. output of the amplifier), at a sampling frequency of 10 kHz. Fig. 4 shows the resultant step response. The voltage of the electromagnet circuit was observed to vary instantly at t=0 s. The output voltage of the load cell-amplifier varied with a time lag, and included a resonance. We identified a transfer function to represent these step response characteristics. The 'transfer function' means a mathematical representation of the relation between the input and output of a linear time-invariant system, generally expressed as a Laplace transform (Franklin et al., 2002). The step response characteristics are usually approximated as a first order or a second order transfer function. We combined these two approximation methods, and expressed the transfer function $M(s)$ as follows:

$$M(s) = \frac{1}{Ts+1} \cdot \frac{\omega_n{}^2}{s^2+2\zeta\omega_n s+\omega_n{}^2} \quad . \tag{1}$$

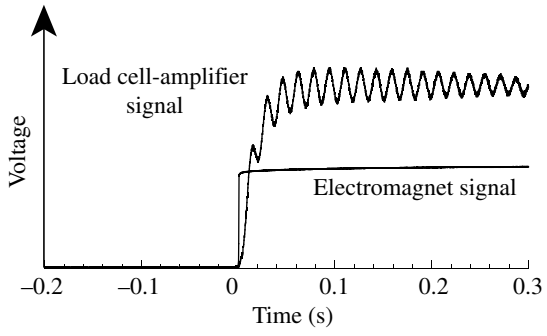

Fig. 4. The resultant voltage variations in the step response measurement. The voltage of the electromagnet circuit varies almost instantly at t=0 s, which determines the time of the step input. The voltage of the load cell-amplifier output varies with a time lag, and includes a resonance.

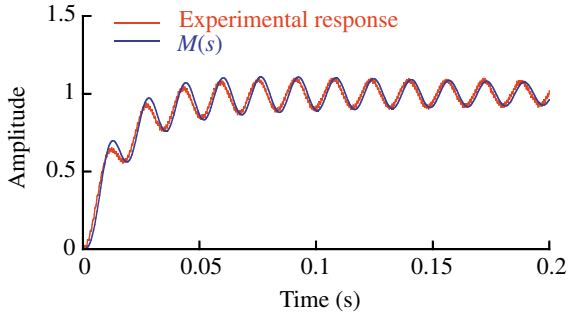

Fig. 5. The step response characteristics of the experimental data and $M(s)$ (Eqn 2). The agreement is observed to be highly reasonable.

Here, T is the time constant, ω_n is the resonance frequency, and ζ is the attenuation coefficient. These parameters were determined through a trial and error process: T=0.016, ω_n=62×2π, and ζ=0.001. Finally, we identified the following transfer function for the force measurement system:

$$M(s) = \frac{9.5\times10^6}{s^3 + 70s^2 + 1.5\times10^5 s + 9.5\times10^6} \cdot \tag{2}$$

The step response characteristics of $M(s)$ were superimposed on the measured step response data in Fig. 5, showing reasonable agreement. The dynamic properties in a frequency domain were also identified from Eqn 2. The frequency response characteristics are, in general, defined as the magnitude and phase differences between the sinusoidal input and output. We can obtain these values at each input frequency by replacing s with $j\omega$ in Eqn 2, where j is the imaginary unit and ω is the input frequency (Franklin et al., 2002). The frequency response characteristics of $M(s)$, calculated by using MATLAB (Mathworks, Natick, MA, USA), are shown in Fig. 6. The style of Fig. 6 is called a 'Bode plot', showing the magnitude and phase differences against logarithmic angular frequency. The frequencies used for the measurements (0.9, 1.8, 3.6 and 7.4 Hz) are equal to 5.6, 11, 22 and 46 rad s^{-1}, respectively (Fig. 6). Fig. 6A shows the magnitude, given as the gain attenuation (G_a) in decibels, according to the following equation:

$$G_a = 20\log\left(\frac{A_{output}}{A_{input}}\right), \tag{3}$$

where A_{input} and A_{output} are the input and output signal amplitudes, respectively. The gain is observed to be attenuated as the frequency increases. Fig. 6B shows the phase differences between the input and output. The phase lag is observed to be enlarged with increasing frequency. We showed the gain attenuation (G_a), attenuation ratio in amplitude (A_{output}/A_{input}), and phase differences (θ_a) at each ω in Table 1. These results indicate that the measurement data obtained by using this force measurement system will include an artifact, which may not be negligible, especially in the high frequency domain. In the analysis of the frequency response of the bumblebees, the

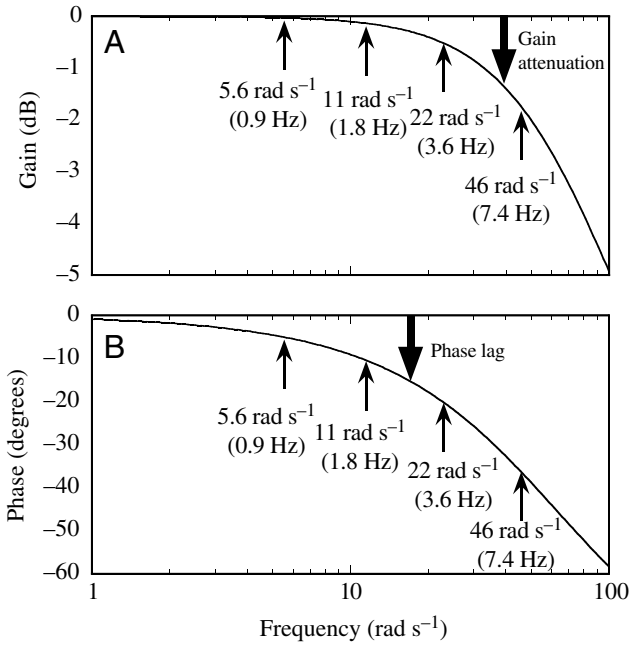

Fig. 6. The frequency response characteristics of our force measurement system, $M(j\omega)$. This style of figure is called a 'Bode plot', and shows the magnitude and phase differences plotted against logarithmic angular frequency. The frequencies used for the measurements (0.9, 1.8, 3.6 and 7.4 Hz) are equal to 5.6, 11, 22 and 46 rad s^{-1}, respectively. (A) The gain in decibels; (B) the phase differences. Note that the gain is attenuated and the phase lag enlarges with increasing frequency, which should be compensated for in the analysis.

values in Table 1 were used to compensate the raw measurement data.

Results

Frequency response of vertical force control

The bumblebees responded to visual oscillations in the vertical direction, and varied their vertical forces. Typical results of the temporal transitions of the vertical force (F_0) and a visual stripe position (z_v) are shown in Fig. 7. The dynamic properties of the force measurement system were not compensated at this stage. The value of F_0 was calculated by dividing the measured force by the weight of the bee, and was equivalent to $\boldsymbol{g}$ in an airplane. The upward direction was defined as the positive direction for both F_0 and z_v. The noticeable fine oscillation in the red lines (F_0), the frequency of which is approximately 150 Hz in common throughout A–D, is most certainly due to the wingbeat of the bumblebee. We removed this unwanted oscillation by using Fourier analysis, and fitted sine curves to the respective F_0 data (broken lines in blue). Fig. 7 shows that the filtered line of F_0 has approximately the same frequency as the line of z_v (bold broken lines in green) at each ω. This indicates that the bumblebees showed the typical frequency response. We focused on their response characteristics in terms of amplitude and phase differences with respect to z_v. In Fig. 7, the amplitude of the force (A_{F_0}) is observed to remain nearly constant, whereas the phase of F_0 (θ_{F_0}) gradually lagged behind that of z_v with increasing ω.

Table 1. *Gain attenuation, amplitude attenuation ratio and phase difference at each stimulation frequency, accompanied by the dynamic force measurements*

ω (rad s^{-1})	G_a (dB)	A_{output}/A_{input}	θ_a (degrees)
5.6	–0.0	1.0	–5
11	–0.1	0.99	–10
22	–0.5	0.95	–20
46	–1.7	0.82	–36

G_a, gain attenuation; A_{output}/A_{input}, amplitude attenuation ratio; θ_a, phase difference; ω, stimulation frequency.

All the results of the responses were summarized with compensations for the dynamic properties of the force measurement system. We defined $\bar{F}_0$ as the compensated force response of the bee, and obtained its frequency response characteristics ($\bar{A}_{F_0}$ and $\bar{\theta}_{F_0}$) according to Table 1 and the following equations:

$$\bar{A}_{F_0} = \frac{A_{F_0}}{A_{output}/A_{input}}, \quad (4)$$

$$\bar{\theta}_{F_0} = \theta_{F_0} - \theta_a . \quad (5)$$

We plotted $\bar{A}_{F_0}$ and $\bar{\theta}_{F_0}$ against a logarithmic frequency axis in Fig. 8. Fig. 8A reveals that most of the $\bar{A}_{F_0}$ data are distributed between 0.1 and 0.5 at each ω, and the mean values are approximately 0.3 in common. The bumblebees did not change $\bar{A}_{F_0}$ distinctly with respect to ω. In contrast, $\bar{\theta}_{F_0}$ clearly decreases with increasing ω (Fig. 8B). When ω is 0.9 and 1.8 Hz (i.e. 5.6 and 11 rad s^{-1}), $\bar{\theta}_{F_0}$ is positive in all the data. Thus, the phase of $\bar{F}_0$ is always earlier than that of z_v. When ω is around 3.6 Hz (i.e. 22 rad s^{-1}), the mean value of $\bar{\theta}_{F_0}$ is approximately 0°, meaning that the phases of $\bar{F}_0$ and z_v are almost synchronized. When ω is 7.4 Hz (i.e. 46 rad s^{-1}), $\bar{\theta}_{F_0}$ is negative in all the data, i.e. the phase of $\bar{F}_0$ lagged behind that of z_v.

Transfer function of visual altitude control system

Although the performance of the visual altitude control system could be partly estimated from Fig. 8, further understanding is difficult to be obtained. This is because the dimensions of the input (z_v) and output ($\bar{F}_0$) are inconsistent. The dimension of the output is in Newtons (or non-dimensionalized), which is a force, whereas that of the input is in mm (a length). When the force measurements are performed under open-loop conditions, the physical values of the input and output can be freely selected. In actual control systems, however, the output is fed back to the input. In order to estimate the direct correlation between the input and output, it is preferable for both the dimensions to be identical. Most of the advanced researches on control engineering have therefore

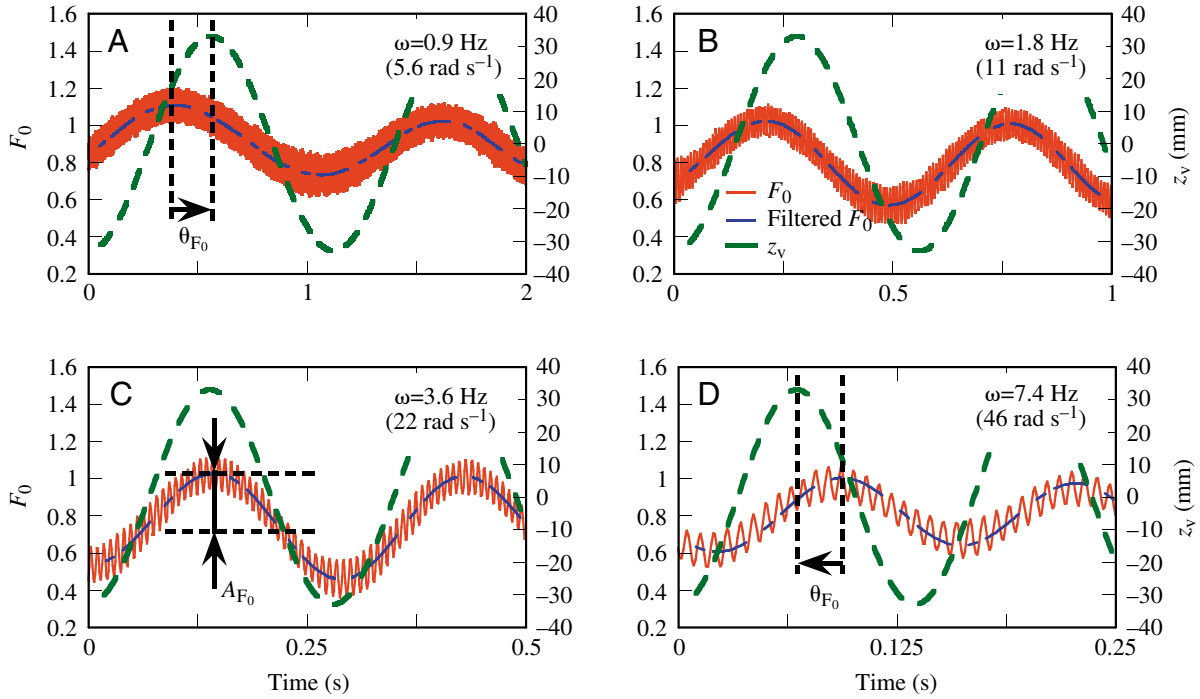

Fig. 7. Typical measurement data of the force response of the bees. The red lines represent the raw measurement data of the vertical force (F_0), without any compensations. The source of fine oscillations in F_0 is certainly the wingbeat of the bee; the oscillation frequency is approximately 150 Hz in common throughout A–D. The broken blue lines represent the filtered data of F_0. The bold broken green lines represent the visual stripe position. The upward direction is defined as the positive direction for both F_0 and z_v. (A) Visual oscillation frequency is 0.9 Hz (5.6 rad s^{-1}). The phase of F_0 obviously precedes that of z_v. (B) Visual oscillation frequency is 1.8 Hz (11 rad s^{-1}). The phase of F_0 still precedes that of z_v. (C) Visual oscillation frequency is 3.6 Hz (22 rad s^{-1}). The phase difference between F_0 and z_v is small. (D) Visual oscillation frequency is 7.4 Hz (46 rad s^{-1}). The phase of F_0 obviously lags behind that of z_v. Although the variation in the phase through A–D is clear, the amplitude of F_0 is relatively constant.

used homogeneous dimension analyses (e.g. Hess and Siwakosit, 2001). In our analysis, we hypothesized that the vertical acceleration was proportional to the measured vertical force, and then calculated the hypothetical vertical position of the bumblebees by integrating the acceleration twice. The equation of motion of a bumblebee in the vertical direction is as follows:

$$m \cdot \ddot{z}_b(t) = mg\bar{F}_0(t) - mg \,, \tag{6}$$

$$\ddot{z}_b(t) = g[\bar{F}_0(t) - 1] \,, \tag{7}$$

where m is the mass of a bumblebee, z_b is the hypothetical vertical position of the bee, $\bar{F}_0$ is the non-dimensional vertical

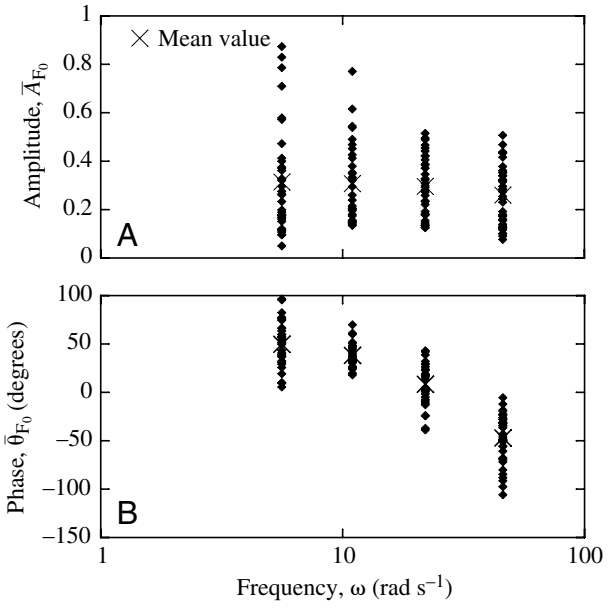

Fig. 8. Summary of all the results of the force response data. The influence of the load cell dynamics was compensated for the respective measurement data, according to Eqn 4 and Eqn 5. We represented the characteristics of the corrected force response ($\bar{F}_0$) in terms of amplitude ($\bar{A}_{F_0}$) and phase ($\bar{\theta}_{F_0}$). (A) $\bar{A}_{F_0}$ is mainly distributed between 0.1 and 0.5 at each ω, and the mean values are approximately 0.3 for all ω. The bumblebees did not change $\bar{A}_{F_0}$ throughout ω. (B) In contrast, $\bar{\theta}_{F_0}$ clearly decreases with increasing ω. When ω is lower than 3.6 Hz (22 rad s^{-1}), $\bar{\theta}_{F_0}$ in all the data is positive, i.e., the phase of $\bar{F}_0$ is earlier than that of z_v. When ω is around 3.6 Hz (22 rad s^{-1}), the mean value of $\bar{\theta}_{F_0}$ is approximately 0°, meaning that the phases of $\bar{F}_0$ and z_v are almost synchronized. When the visual stripes oscillate at 7.4 Hz (46 rad s^{-1}), $\bar{\theta}_{F_0}$ in all the data is negative, i.e. the phase of $\bar{F}_0$ lagged behind that of z_v.

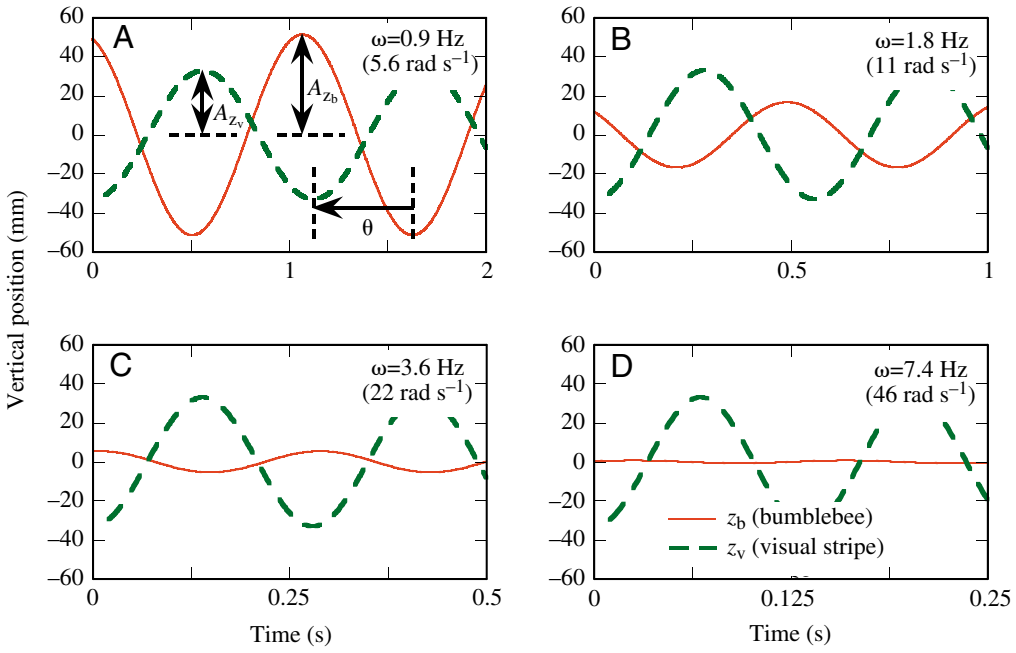

Fig. 9. Typical results for the position response of the bees. We obtained the hypothetical variation in position of the bees (z_b, red lines) according to Eqn 7. The bold broken green lines represent the visual stripe position (z_v). We focused on the amplitudes of z_b (A_{z_b}) and z_v (A_{z_v}), and the phase differences between z_b and z_v (θ). (A) When ω=0.9 Hz (5.6 rad s^{-1}), A_{z_b} is larger than A_{z_v}, and θ is larger than –180°. (B) When ω=1.8 Hz (11 rad s^{-1}), A_{z_b} is a little smaller than A_{z_v}, and θ is larger than –180°. (C) When ω=3.6 Hz (22 rad s^{-1}), A_{z_b} becomes much smaller than A_{z_v}, and θ is approximately –180°. (D) When ω=7.4 Hz (46 rad s^{-1}), the oscillation in z_b is hardly perceptible. The value of θ is, in fact, much smaller than –180°.

force, and $\boldsymbol{g}$ is the acceleration of gravity. Because the mean value of $\bar{F}_0$ is generally not equal to 1, direct solution of Eqn 7 involves acceleration motion, which is unnecessary for the frequency response analysis. To avoid this problem, we added an appropriate constant to the right side of Eqn 7, and solved the differential equation. As a result, the input parameter was the vertical position of the visual stripes, z_v, and the output was the hypothetical vertical position of the bee, z_b. Fig. 9 shows typical results of the correlation between z_v and z_b at each ω. The lines in red represent z_b, and the bold broken lines in green represent z_v. We defined A_{z_b} and A_{z_v} as amplitudes of z_b and z_v, respectively, and θ as phase difference between z_b and z_v. As shown in Fig. 9A–D, A_{z_b} is clearly attenuated, and that θ decreases with increasing ω.

We summarized all the results on a Bode plot (Fig. 10). Fig. 10A shows the gain of the system (G), calculated by the following equation:

$$G = 20\log\left(\frac{A_{z_b}}{A_{z_v}}\right). \quad (8)$$

Fig. 10B shows the phase differences (θ). The mean values of G and θ at each ω are shown in Table 2. These values were used for identifying the transfer function of the visual altitude control system. Because the sets of G and θ were obtained at only four frequencies, the number of representable expressions of the transfer function were infinite. Therefore, we focused on finding the simplest expression by means of the following two steps.

First, we hypothesized that the transfer function $B(s)$ was represented as a product of a linear part and a non-linear exponential part:

$$B(s) = B_0(s)\cdot e^{-\tau_e s}. \quad (9)$$

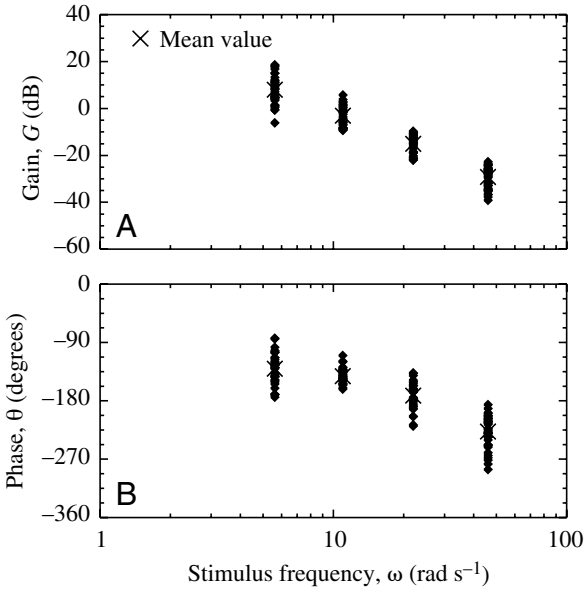

Fig. 10. All the results of the position response of the bees were summarized on a Bode plot. (A) Gain of the response (G), calculated from Eqn 8. (B) Phase differences between z_b and z_v (θ). The gain is attenuated at approximately –40 dB/decade. The phase lag is observed to enlarge with increasing frequency.

This hypothesis is based on an earlier study (McRuer and Graham, 1964), in which a transfer function of human systems was simply approximated as a style of Eqn 9. The exponential part means a time delay of the system, mostly due to transport delays and high frequency neuromuscular lags in animals. In insect motion, effective time delay τ_e is approximately a few dozen ms (Azuma, 1992; Höltje and Hustert, 2003; Ridgel et

Table 2. *Gain and phase difference of open-loop transfer function [(B(s)] at each stimulation frequency*

ω (rad s^{-1})	G (dB)	θ (degrees)
5.6	7.8	–130
11	–3.3	–142
22	–15.4	–172
46	–29.6	–227

G, gain; θ, phase difference; ω, stimulation frequency.

Table 3. *Gain and phase difference of bumblebee exponential frequency response at each stimulation frequency*

ω (rad s^{-1})	G_e (dB)	θ_e (degrees)
5.6	0.0	–6
11	0.0	–12
22	0.0	–25
46	0.0	–53

G_e, gain; θ_e, phase difference of exponential frequency response $e^{-\tau_e s}$; ω, stimulation frequency.

al., 2001). We hypothesized that τ_e for the bumblebees was 0.02 s. The frequency response characteristics of $e^{-\tau_e s}$ are remarkable in that the gain is 0 dB throughout the frequency domain, whereas the phase lag enlarges with increasing frequency. We showed the gain (G_e) and the phase (θ_e) of $e^{-\tau_e s}$ at each measured ω in Table 3. Here, we benefit from using the Bode plot, in which the gain is expressed on a logarithmic scale, and the phase is expressed on a linear scale. In this case, the frequency response characteristics (i.e. gain and phase difference) of an arbitrary transfer function, $T(s)=T_1(s)T_2(s)\ldots T_n(s)$, are calculated as the summation of those of $T_1(s)$, $T_2(s)$, …, and $T_n(s)$. For example, the gain and phase of $B(s)$ can be calculated as follows:

$$G = G_0 + G_e \,, \tag{10}$$

and

$$\theta = \theta_0 + \theta_e \,, \tag{11}$$

where G_0 and θ_0 are the gain and phase of $B_0(s)$, respectively. We can, therefore, identify the frequency response characteristics of $B_0(s)$ by subtracting those of $e^{-\tau_e s}$ from those of $B(s)$. We showed the resultant values of G_0 and θ_0 in Table 4.

Table 4. *Gain and phase difference of bumblebee open-loop transfer function at each stimulation frequency*

ω (rad s^{-1})	G_0 (dB)	θ_0 (degrees)
5.6	7.8	–124
11	–3.3	–130
22	–15.4	–147
46	–29.6	–174

G_0, gain; θ_0, phase difference of open-loop transfer function $B_0(s)$; ω, stimulation frequency.

Next, we determined the expression of $B_0(s)$. The Bode plot is useful again in finding the simplest expression. In Fig. 10, the slope of the gain curve is observed to be approximately –40 dB/decade, which should be identical to that of $B_0(s)$. In general, the gain slope becomes steeper by –20 dB/decade per a power of $1/s$ in a Bode plot (Franklin et al., 2002). This indicates that $1/s^2$ is dominant in $B_0(s)$. Therefore, the simplest expression of $B_0(s)$, around the measured frequency domain, is represented as follows:

$$B_0(s) = \frac{a}{s^2+bs+c} \,. \tag{12}$$

Each coefficient (a, b and c) in Eqn 12 was calculated by a MATLAB program, using an algorithm of identifying continuous-time filter parameters from frequency response data. The resultant $B_0(s)$ was:

$$B_0(s) = \frac{79}{s^2+6s+16} \,. \tag{13}$$

Consequently, the transfer function of the visual altitude control system in the bumblebees is represented as:

$$B(s) = \frac{79}{s^2+6s+16} \cdot e^{-0.02s} \,, \tag{14}$$

$$\approx \left(\frac{9}{s+3}\right)^2 e^{-0.02s} \,. \tag{15}$$

In Fig. 11, the frequency responses of $B_0(s)$ and $B(s)$ [i.e. $B_0(j\omega)$ and $B(j\omega)$, respectively] were shown with the measurement data. The agreement between $B(s)$ and the measurement data is observed to be reasonable in both G and θ.

Discussion

The frequency response characteristics of visual altitude control system were measured for bumblebees. The tethered bumblebees responded to visual oscillations in the vertical direction, and varied their vertical forces (F_0) according to the oscillation frequency (ω). We measured the temporal transitions of F_0 at each ω (0.9, 1.8, 3.6 and 7.4 Hz) (Fig. 8). Because the raw measurement data included an artifact due to the dynamics of the force measurement system, we compensated the data for the influence of the artifact, and obtained corrected force response of the bees ($\bar{F}_0$).

The frequency responses have been studied for other insects. Sherman and Dickinson (Sherman and Dickinson, 2003) measured the frequency response of fruit flies *Drosophila melanogaster* by mechanically and visually oscillating the tethered flies about the pitch, roll and yaw axes, and recorded the changes in wingbeat amplitude and wingbeat frequency. They characterized the dynamics of the visual and mechanosensory systems, and revealed that both feedback systems were composed of band-pass filters of different

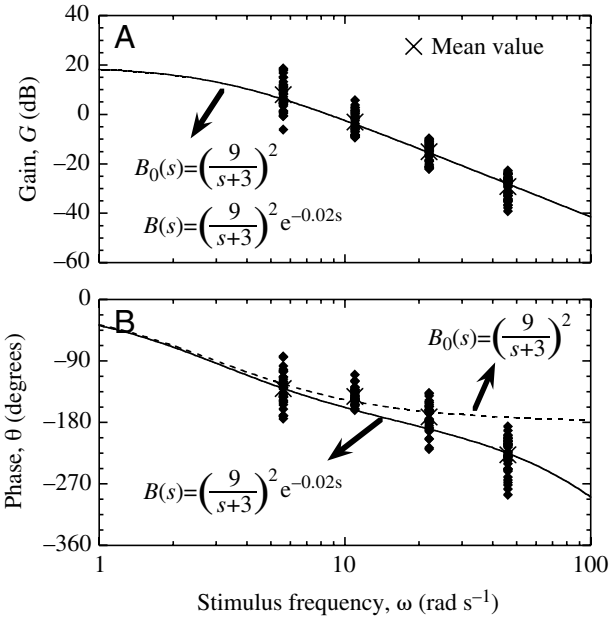

Fig. 11. The measured response data fitted with a transfer function, derived from a hypothesis that the expression was a product of a linear part and a non-linear exponential part. The exponential part affects the phase lags only (see solid and broken lines). We obtained the simplest transfer function: $B(s)=[9/(s+3)]^2e^{-0.02s}$. It is observed that $B(s)$ fits well for both the gain and phase data.

frequency characteristics. In a subsequent study, they also successfully identified the contribution of each sensory modality (Sherman and Dickinson, 2004).

In our study, we focused on the variations in amplitude and phase of the frequency response for visual altitude control. Our results showed that the amplitude ($\bar{A}_{F_0}$) was almost constant, and that the phase ($\bar{\theta}_{F_0}$) gradually lagged with increasing ω (Fig. 8). Next, we solved the equation of motion (Eqn 7) to obtain variations in hypothetical vertical position of the bee. For the purpose of adjusting the dimensions of the input and output, we defined the input parameter as the vertical position of the visual stripes (z_v) and the output as the hypothetical vertical position of the bumblebee (z_b). Fig. 9 shows that the amplitude of z_b is clearly attenuated, and that the phase of z_b lagged with increasing ω. We summarized all the results on a Bode plot (Fig. 10). The simplest transfer function, representing the frequency response characteristics of the bumblebees, was obtained as Eqn 15.

Influence of compensations for the load cell dynamics

We measured the dynamic response of the bumblebees by using a load cell. The raw measurement data, however, included an artifact due to the load cell dynamics, which should be compensated for in the analysis. We identified these dynamic properties by measuring the step response of the force measurement system (Figs 3, 4). We represented the step response characteristics by using a transfer function, $M(s)$ (Eqn 1), and estimated the gain attenuation and phase lags in the frequency domain, on the basis of $M(s)$ (Fig. 6 and Table 1). These dynamic properties were compensated for in the analysis of the vertical force data of the bees, according to Eqn 4, 5. As shown in Fig. 6 and Table 1, the influence of the artifact enlarges with increasing frequency. In other words, the data corrections we performed may have importance in the high frequency domain. Here, we discuss how the compensation affected our frequency response analysis.

First, we focus on the gain control analysis. The maximum of the gain attenuation due to the load cell dynamics is 1.7 dB at ω=46 rad s^{-1} (Table 1). This is much smaller than the gain variation through ω (from 7.8 to –29.6 dB) (Table 2). We notify that the correction values in gain included in the position response data are also equal to G_a. The compensations performed for the gain results, therefore, had little influence on our analysis. On the other hand, phase lags caused by the load cell dynamics are not negligible. When ω is 22 or 46 rad s^{-1}, the phase lags due to the artifact are more than 10% of the lags in the response of the bees (Tables 1, 2). The influence of the compensations was more significant for the phase analysis, rather than for the gain analysis.

As a result of performing the compensations for the measurement data, the phase lags decreased whereas the gain was almost unchanged. It is naturally desirable for the stable control to have smaller phase lags. This indicates that the data with the compensations show more stable control characteristics than the data without the compensations. We discuss the dynamic stability in the visual altitude control system of the bumblebees in the subsequent section ('Meaning of the obtained transfer function'), on the basis of the gain and phase characteristics. We define an indicator of the dynamic stability, 'stability margin' in that section. We will see with ease that the smaller phase lags contribute to the larger stability margin.

Visual perception and flight control in the bumblebees

We utilized the sensitivity for image motion in bumblebees, and elicited flight modulation in the vertical direction. Recent studies have revealed that flying insects use cues derived from optic flow for navigational purposes (e.g. Srinivasan et al., 1996). For example, bees flying through a tunnel maintain equidistance from the flanking walls by balancing the apparent speeds of the images of the walls (Kirchner, 1989; Srinivasan et al., 1996). Bees landing on a horizontal surface hold constant the image velocity of the surface as they approach it (Srinivasan et al., 2000; Srinivasan et al., 1996). A large number of studies have focused on modeling the visual motion detection mechanisms of insects, which have been summarized (Srinivasan et al., 1999). Neumann and Bülthoff showed successful simulations of visual flight control by using these models (Neumann and Bülthoff, 2000; Neumann and Bülthoff, 2001; Neumann and Bülthoff, 2002).

The motion-sensitive mechanism in an insect measures the angular velocity of the moving image (Srinivasan et al., 1996). Therefore, the bumblebees used in our experiments most certainly responded to the variation in the angular velocity of

the stripes, rather than the position of the stripes. This indicates that the transfer function (Eqn 15), obtained in the positional dimension, is also likely dependent on the angular velocity. In the process of finding Eqn 15, we focused on the amplitude and phase of the hypothetical position of the bee with respect to those of the stripe position. Even though A_{z_v} (amplitude of the visual oscillation) is given as a constant, the angular velocity perceived by the bee varies according to the distance between the bee and the display. This implies that the resultant transfer function, $B(s)$, is applicable within the framework of the present experimental conditions. However, the applicable range is likely rather extensive, because the amplitude of the response is dealt with in a logarithmic scale.

We analyzed the bumblebee's control system in the dimension of position, for the purpose of evaluating its control characteristics from the viewpoint of human-related control systems. Human beings can perceive structure and position of a stationary object with high accuracy. Therefore, human beings are most likely to guide their movement by using position control (Rushton et al., 1998), although they also seem to use the optic flow as well (Warren et al., 2001). On the other hand, insects have inferior spatial acuity in comparison with human beings (Horridge, 1977). The insects achieve the same tasks only by using the optic flow. Insects and human beings, therefore, respond to different elements of image motion; insects primarily respond to the velocity, whereas human beings primarily respond to the position. However, we can compare their frequency response characteristics in the same framework of analysis. This is because the available transfer functions for the frequency response are identical, whether they are calculated in the dimension of velocity or position, as far as both the sinusoidal input and output have the same dimension. In addition, the purpose of controlling their motion is the same: reliable guidance to a destination. We can therefore estimate the control performance of the bumblebee system by using Eqn 15, in the same manner as the control analysis for human systems. Below, we discuss the control stability of the bumblebee system, and differences between the bumblebee and a human pilot-vehicle system, on the basis of the resultant transfer function (Eqn 15).

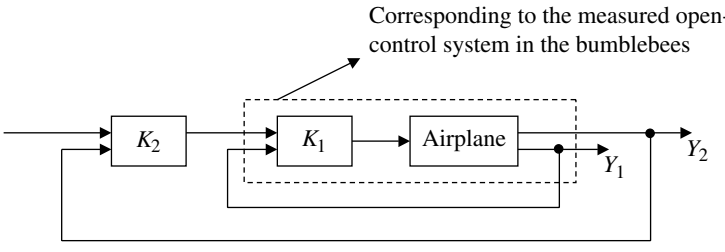

Fig. 12. Block diagram of a typical flight control system of airplanes. The inside loop including K_1 is called a 'stabilization control loop'. This K_1 loop controls quick responses reflexively. The outside loop including K_2 is called a 'guidance and navigation control loop'. The K_2 loop controls relatively slow responses such as selection of a flight course. This K_2 loop is likely comparable to the system that conveys an intention in the bees. The reflexive responses measured in our study are most likely corresponding to the output of the K_1 loop, Y_1.

Meaning of the obtained transfer function

In this study, the visual stripes were oscillated in the open-loop condition. The tethered bumblebees could not feed back the variation in the vertical force to the stripe position. The results therefore do not represent the will of the bees to optimize their entire flight, but most certainly represent the conditional reflexes at each instant. For the purpose of characterizing this reflexive response of the bees, we utilized a model of an airplane control system. Fig. 12 shows a block diagram of the most advanced control system in airplanes (Mclean, 1990; McRuer, 1973). The inside loop including K_1 is called the 'stabilization control loop'. SAS (Stability Augmentation System) and CAS (Control Augmentation System) are examples of such loops. This K_1 loop reflexively controls quick responses. The outside loop including K_2 is called the 'guidance and navigation control loop'. A typical example of this loop is the automatic flight control system consisting of TMS (Thrust Management System) and FMS (Flight Management System). The K_2 loop controls relatively slow responses. We applied this control model to the measured bumblebee system. The K_2 loop in Fig. 12 is likely comparable to the system that conveys an intention in the bees (for example, an intention to reach the destination as soon as possible, or an intention to fly as far away as possible). The reflexive response measured in our study is most likely corresponding to the open-loop output of the K_1 loop, Y_1 in Fig. 12.

The performance of this reflexive control system in the bumblebees can be estimated on the basis of the frequency response results. When we analyze control characteristics of an open-loop system, 'crossover frequency' and 'stability margin' are important (Franklin et al., 2002). The crossover frequency is, in general, divided into the gain crossover frequency and the phase crossover frequency. The stability margin is also divided into the gain margin and the phase margin. The gain crossover frequency (ω_{gc}) is defined as the frequency that produces a gain of 0 dB. The phase crossover frequency (ω_{pc}) is defined as the frequency that produces a phase of –180°. The gain margin (GM) is the difference between the gain curve and 0 dB at ω_{pc}. The phase margin (PM) is the difference in phase between the phase curve and –180° at ω_{gc}. Each of ω_{gc}, ω_{pc}, GM, and PM in our measurement data are shown in Fig. 13, revealing that the measured bumblebee system has sufficient stability margins for both gain and phase. When PM is less than 90°, ω_{gc} is less than or equal to the bandwidth, ω_{bw} (Franklin et al., 2002). The bandwidth is defined as the frequency at which the gain in the closed-loop response is attenuated 3 dB from the steady state. Larger ω_{bw} means that the output of the closed-loop control system can follow the input up to higher frequencies. In other words, larger ω_{gc} yields larger ω_{bw}, and the quick response characteristics are improved. In addition, PM is

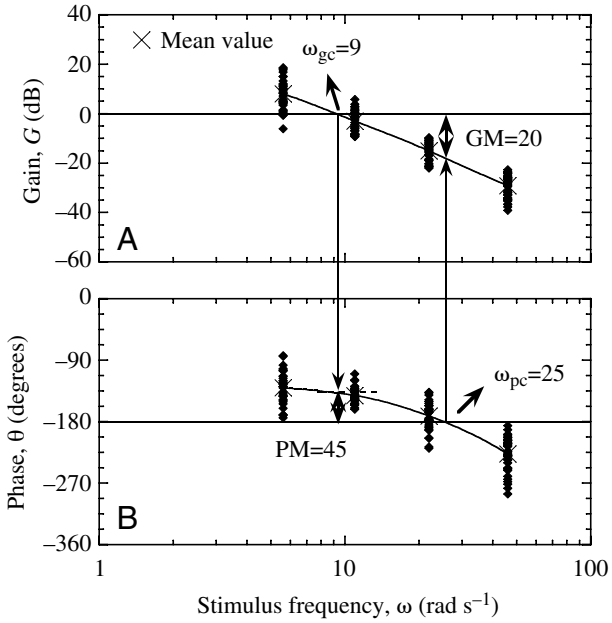

Fig. 13. Gain crossover frequency (ω_{gc}), phase crossover frequency (ω_{pc}), gain margin (GM), and phase margin (PM) of the measured bumblebee system. ω_{gc} is defined as the frequency that produces a gain of 0 dB, and ω_{pc} as the frequency that produces a phase of –180°. GM is the difference between the gain curve and 0 dB at ω_{pc}, and PM is the difference in phase between the phase curve and –180° at ω_{gc}. The dynamic stability of a control system can be quantified on the basis of GM and PM. When both GM and PM are positive, the control system is dynamically stable. Our results (GM~20 and PM~45) indicate that the measured bumblebee system has substantial dynamic stability.

known as an indicator of damping characteristics; larger PM yields a smaller peak gain in a closed-loop control system (Franklin et al., 2002).

Empirical studies guide designers of control systems in their choice for PM and GM values. In the case of designing a servo control system, for example, output should be controlled to track a target value, and PM of 40~60° and GM of 10~20 dB are desirable. In the case of designing a regulator control system, on the other hand, output should be kept constant to minimize the effect of disturbances, and PM larger than 20° and GM of 3~10 dB are required. In Fig. 13, it is observed that ω_{gc}=9 rad s^{-1}, ω_{pc}=25 rad s^{-1}, GM=20 dB and PM=45°. These results indicate that the measured control system in the bumblebees is analogous to an ideal servo control system.

Comparison between human beings and bumblebees in terms of dynamic control characteristics

Dynamic flight control analysis has long been studied in the field of aeronautical engineering. McRuer and Graham (McRuer and Graham, 1964) studied the dynamic control characteristics of a human pilot operating an aerospace vehicle. They analyzed the frequency response of the human pilot, and revealed that the open-loop control characteristics of the combined system (human pilot-vehicle system) can be approximated by using a simple transfer function. This transfer function model is called 'the crossover model', and is represented as the following expression, where H_p and H_c mean the describing functions of the human pilot and the controlled element (vehicle), respectively:

$$H(j\omega) = H_p H_c \approx \frac{\omega_{gc} e^{-j\omega\tau_e}}{j\omega} \text{ ; near } \omega_{gc} . \quad (16)$$

The crossover frequency, ω_{gc}, is equivalent to the loop gain, and accounts for the adaptive compensation of the pilot for the controlled element gain. An effective time delay, τ_e, includes the lags due to transport delays and high frequency neuromuscular dynamics. In general, τ_e is approximately 0.2 s in humans, ten times larger than in the bumblebees. The simplest describing function of the pilot is represented as follows:

$$H_p = K_p \frac{T_L j\omega + 1}{T_I j\omega + 1} e^{-j\omega\tau_e} , \quad (17)$$

where K_p is pilot static gain, T_L is lead time constant, and T_I is lag time constant. Eqn 17 indicates that the human pilot can be adjusted for variation in lead-lag characteristics of the controlled element by modifying T_L and T_I, so as to keep 'the crossover model'. Although more complicated and fitted models have been developed (e.g. Davidson and Schmidt, 1992; Kleinman et al., 1970), the crossover model is still widely accepted among researchers of man-machine interfaces.

McRuer and Graham proposed design guidance for vehicle systems, on the basis of the crossover model. They suggested that an appropriate vehicle system needs PM of approximately 40°, and that the gain slope near ω_{gc} on a Bode plot should be –20 dB/decade. Because PM is directly correlated with the dynamic stability, the requirement for PM is principal in designing the system. The requirement for the gain slope is derived from the crossover model, because 1/*s* gives a gain slope of –20 dB/decade. If the system is designed to satisfy these conditions, the human pilot does not need to compensate for the dynamics of the vehicle system, and the handling quality is improved. However, the both requirements for PM and gain slope are simultaneously satisfied under limited condition, because the gain and phase characteristics of a system are correlated with each other (Franklin et al., 2002). When the gain slope becomes steeper, the phase lag inevitably enlarges, and the positive phase margin may be lost.

We compared the control characteristics of the measured bumblebee system with the crossover model. The frequency response data of the two systems are shown in Fig. 14. The data of the human pilot-vehicle system were quoted from McRuer and Jex (McRuer and Jex, 1967). Our results reveal that the gain slope is approximately –40 dB/decade in the bumblebee response, whereas it is approximately –20 dB/decade in the human response. Considering that the measured bumblebee system is prominently dominated by the effect of $(\omega_{gc}/s)^2$ (because ω_{gc}~9), the control rule in the visual altitude control system of the bumblebee could be called as 'the square

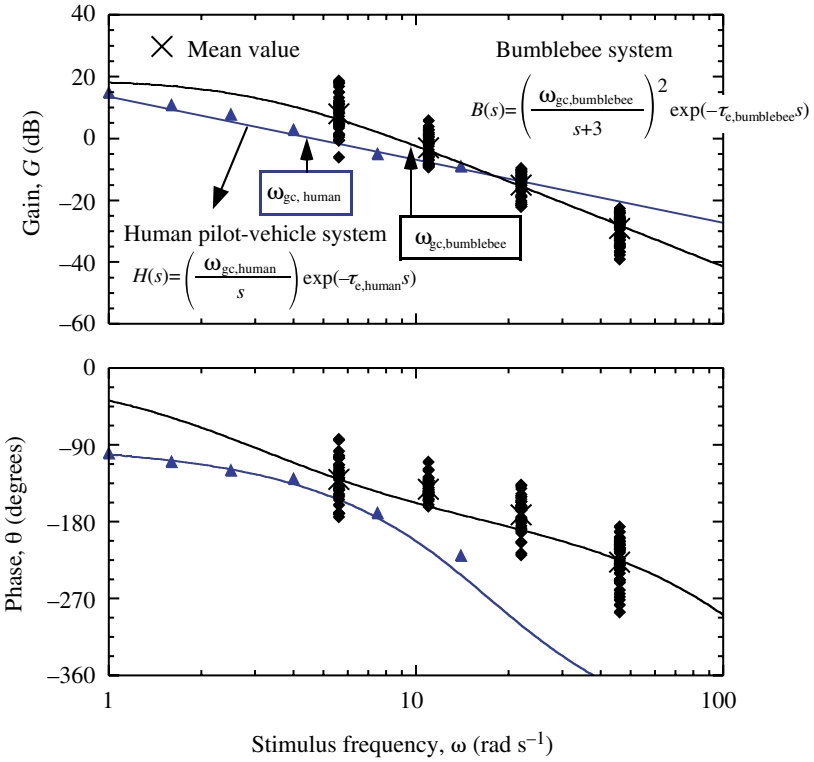

Fig. 14. The measured control characteristics of the bumblebee system are compared with the characteristics of a human pilot-vehicle system (McRuer and Jex, 1967). For the human system, the control characteristics are fitted with a transfer function, $H(s)=\omega_{gc,human}/s\cdot e^{-\tau e,humans}$ (the crossover model). On the other hand, the control characteristics in the bumblebee system can be approximated as $B(s)=[\omega_{gc,bumblebee}/(s+3)]^2\cdot e^{-\tau e,bumblebees}$, which could be called 'the square crossover model'. The bumblebee system is observed to possess higher gain at $\omega<\omega_{gc}$ than the human system, indicating higher performance in terms of the steady-state characteristics. The gain crossover frequency in the bumblebee system ($\omega_{gc,bumblebee}$) is approximately twice as large as that in the human pilot-vehicle system ($\omega_{gc,human}$). Because larger ω_{gc} causes larger bandwidth in the system, the bumblebee system is revealed to possess superior quick response characteristics. We already verified that the bumblebee system possesses substantial phase margin (PM; Fig. 13), indicating that the system possesses excellent damping characteristics. The bumblebee system was, therefore, revealed to have superiority in terms of the steady-state and transient (i.e. quick response and damping) characteristics, in comparison with the human pilot-vehicle system.

crossover model'. Because the bumblebee system possesses a steeper gain slope than the human pilot-vehicle system, the gain at $\omega<\omega_{gc}$ is higher in the bumblebee system than in the human pilot-vehicle system. The behavior at low frequencies generally determines the attenuation of disturbances and the performance of tracking low frequency reference signals. These are called steady-state characteristics, and high gain is required to improve these characteristics. The measured control system in the bumblebee is, therefore, revealed to possess superior steady-state characteristics in comparison with the human pilot-vehicle system. The steeper gain slope also produces lower gain at high frequencies. Such behavior is desirable because the robust stability, which is more important than the attenuation of disturbances at high frequencies, is improved.

Evaluation of the control performance must also include the transient characteristics as well as the steady-state characteristics. The transient characteristics are divided into damping characteristics and quick response characteristics. The adequate PM in the bumblebee system indicates excellent damping characteristics, which are comparable to those of an ideal control system for humans. The quick response characteristics depend on the gain crossover frequency. In a human pilot-vehicle system, the gain crossover frequency ($\omega_{gc,human}$) is roughly 2–5 rad s^{-1} (McRuer and Jex, 1967), which is approximately half of the gain crossover frequency in the measured bumblebee system ($\omega_{gc,bumblebee}$). The bumblebee system is, therefore, revealed to possess superior quick response characteristics in comparison with the human pilot-vehicle system.

In conclusion, we have measured and analyzed the frequency response characteristics of visual altitude control system in the bumblebees. The measured bumblebee system is revealed to have superiority in both the steady-state and transient characteristics, in comparison with the human pilot-vehicle system. Such excellence will be the evidence that the bumblebees can effectively control their flight with stability and maneuverability.

List of abbreviations and symbols

A	amplitude
A_{F_2}	raw amplitude of force response
$\overline{A}_{F_2}$	corrected amplitude of force response
A_{z_b}	amplitude of position response
A_{z_v}	amplitude of visual oscillation
$B(s)$	open-loop transfer function of bumblebee
B_0	linear part of $B(s)$
F_0	non-dimensional raw vertical force
$\overline{F}_0$	non-dimensional corrected vertical force
$\boldsymbol{g}$	acceleration of gravity
G	gain
G_a	gain attenuation
G_0	gain of $B_0(s)$
GM	gain margin
H	open-loop transfer function of human pilot-vehicle system
H_c	describing function of controlled element in human pilot-vehicle system
H_p	describing function of human pilot
j	imaginary unit

K_p	pilot static gain
m	mass of bumblebee
$M(s)$	transfer function of force measurement system
PM	phase margin
s	parameter in Laplace transform
t	time
T	time constant
T_I	lag-time constant
T_L	lead-time constant
z_b	hypothetical vertical position of bumblebee
z_v	vertical position of visual stripes
ζ	attenuation coefficient
θ	phase
θ_{F_0}	raw phase of force response
$\bar{\theta}_{F_0}$	corrected phase of force response
θ_0	phase of $B_0(s)$
τ_e	effective time delay
ω	input frequency (stimulus frequency)
ω_{bw}	bandwidth
ω_{gc}	gain crossover frequency
ω_n	resonance frequency
ω_{pc}	phase crossover frequency

The present work was supported in part through the 21st Century COE Program, 'Mechanical Systems Innovation', and Grant-in-Aid for Scientific Research (S), 18100002, 2006, by the Ministry of Education, Culture, Sports, Science and Technology, Japan.

References

Azuma, A. (1992). *The Biokinetics of Flying and Swimming*. Tokyo: Springer-Verlag.

Davidson, J. B. and Schmidt, D. K. (1992). Modified optimal control pilot model for computer-aided design and analysis. *NASA-TM-4386*.

Franklin, G. F., Powell, J. D. and Emami-Naeini, A. (2002). *Feedback Control of Dynamic Systems*. Upper Saddle River, NJ: Prentice Hall.

Götz, K. G. and Wehrhahn, C. (1984). Optomotor control of the force of flight in *Drosophila* and *Musca*. *Biol. Cybern.* **51**, 129-134.

Hess, R. A. and Siwakosit, W. (2001). Assessment of flight simulator fidelity in multiaxis tasks including visual cue quality. *J. Aircraft* **38**, 607-614.

Höltje, M. and Hustert, R. (2003). Rapid mechano-sensory pathways code leg impact and elicit very rapid reflexes in insects. *J. Exp. Biol.* **206**, 2715-2724.

Horridge, G. A. (1977). Insects which turn and look. *Endeavour* **NS1**, 7-17.

Kirchner, W. H. (1989). Freely flying honeybees use image motion to estimate object distance. *Naturwissenschaften* **76**, 281-282.

Kleinman, D. L., Baron, S. and Levison, W. H. (1970). An optimal control model of human response. Part I: theory and validation. *Automatica* **6**, 357-369.

Lehmann, F.-O. and Dickinson, M. H. (1997). The changes in power requirements and muscle efficiency during elevated force production in the fruit fly *Drosophila melanogaster*. *J. Exp. Biol.* **200**, 1133-1143.

Lehmann, F.-O. and Dickinson, M. H. (1998). The control of wing kinematics and flight forces in fruit flies (*Drosophila* spp.). *J. Exp. Biol.* **201**, 385-401.

Mclean, D. (1990). *Automatic Flight Control Systems*. Upper Saddle River, NJ: Prentice Hall.

McRuer, D. T. (1973). *Aircraft Dynamics and Automatic Control*. Princeton: Princeton University Press.

McRuer, D. T. and Graham, D. (1964). Pilot-vehicle control system analysis. In *Guidance and Control*. Vol. 2 (ed. R. C. Langford and C. J. Mundo), pp. 603-621. New York: Academic Press.

McRuer, D. T. and Jex, H. R. (1967). A review of Quasi-linear pilot models. *IEEE Trans. Hum. Factors Electron.* **8**, 231-249.

Neumann, T. R. and Bülthoff, H. H. (2000). Biologically motivated visual control of attitude and altitude in translatory flight. In *Artificial Intelligence, Proceedings of the 3rd Workshop 'Dynamische Perzeption'*. Vol. 9 (ed. G. Baratoff and H. Neumann), pp. 135-140. Berlin: Infix-Verlag.

Neumann, T. R. and Bülthoff, H. H. (2001). Insect inspired visual control of translatory flight. In *Advances in Artificial Life, Proceedings of ECAL*. Vol. 2159 (ed. J. Kelemen and P. Sosik), pp. 627-636. Berlin: Springer-Verlag.

Neumann, T. R. and Bülthoff, H. H. (2002). Behavior-oriented vision for biomimetic flight control. In *Proceedings of the EPSRC/BBSRC International Workshop on Biologically Inspired Robotics: The Legacy of W. Grey Walter*, pp. 196-203. HP Labs: Bristol, UK.

Ridgel, A. L., Frazier, F. S. and Zill, S. N. (2001). Dynamic responses of tibial campaniform sensilla studied by substrate displacement in freely moving cockroaches. *J. Comp. Physiol. A* **187**, 405-420.

Rushton, S. K., Harris, J. M., Lloyd, M. R. and Wann, J. P. (1998). Guidance of locomotion on foot uses perceived target location rather than optic flow. *Curr. Biol.* **8**, 1191-1194.

Sane, S. P. (2003). The aerodynamics of insect flight. *J. Exp. Biol.* **206**, 4191-4208.

Sherman, A. and Dickinson, M. H. (2003). A comparison of visual and haltere-mediated equilibrium reflexes in the fruit fly *Drosophila melanogaster*. *J. Exp. Biol.* **206**, 295-302.

Sherman, A. and Dickinson, M. H. (2004). Summation of visual and mechanosensory feedback in *Drosophila* flight control. *J. Exp. Biol.* **207**, 133-142.

Spaethe, J. and Chittka, L. (2003). Inter individual variation of eye optics and single object resolution in bumblebees. *J. Exp. Biol.* **206**, 3447-3453.

Srinivasan, M. V., Zhang, S. W., Lehrer, M. and Collett, T. S. (1996). Honeybee navigation *en route* to the goal: visual flight control and odometry. *J. Exp. Biol.* **199**, 237-244.

Srinivasan, M. V., Poteser, M. and Kral, K. (1999). Motion detection in insect orientation and navigation. *Vis. Res.* **39**, 2749-2766.

Srinivasan, M. V., Zhang, S. W., Chahl, J. S., Barth, E. and Venkatesh, S. (2000). How honeybees make grazing landings on flat surfaces. *Biol. Cybern.* **83**, 171-183.

Sun, M. and Xiong, Y. (2005). Dynamic flight stability of a hovering bumblebee. *J. Exp. Biol.* **208**, 447-459.

Taylor, G. K. and Thomas, A. L. R. (2003). Dynamic flight stability in the desert locust *Schistocerca gregaria*. *J. Exp. Biol.* **206**, 2803-2829.

Warren, W. H., Kay, B. A., Zosh, W. D., Duchon, A. P. and Sahuc, S. (2001). Optic flow is used to control human walking. *Nat. Neurosci.* **4**, 213-216.